


Control of ternary alloy composition during remote epitaxy on graphene

Zachary LaDuca, Katherine Su, Sebastian Manzo, Michael S. Arnold, and Jason K. Kawasaki^{*}
Materials Science and Engineering, University of Wisconsin-Madison, Madison, Wisconsin 53706, USA

 (Received 22 May 2023; accepted 24 July 2023; published 10 August 2023)

Understanding the sticking coefficient σ , i.e., the probability of an adatom sticking to a surface, is essential for controlling the stoichiometry during epitaxial film growth. However, σ on monolayer graphene-covered surfaces and its impact on remote epitaxy are not understood. Here, using molecular-beam epitaxial growth of the magnetic shape memory alloy Ni_2MnGa , we show that the sticking coefficients for metals on graphene-covered MgO (001) are less than one and are temperature and element dependent, as revealed by ion backscattering spectrometry and energy-dispersive x-ray spectroscopy. This lies in stark contrast with most transition metals sticking on semiconductor and oxide substrates, for which σ is near unity at typical growth temperatures ($T < 800^\circ\text{C}$). By initiating growth below 400°C , where the sticking coefficients are closer to unity and wetting on the graphene surface is improved, we demonstrate the epitaxy of Ni_2MnGa films with controlled stoichiometry that can be exfoliated to produce freestanding membranes. Straining these membranes tunes the magnetic coercive field. Our results provide a route to synthesize membranes with complex stoichiometries whose properties can be manipulated via strain.

DOI: [10.1103/PhysRevMaterials.7.083401](https://doi.org/10.1103/PhysRevMaterials.7.083401)

I. INTRODUCTION

Remote [1,2] and van der Waals [3–6] epitaxy on monolayer graphene-covered substrates are promising strategies for synthesizing single-crystalline films that are mechanically decoupled from the substrate. In remote epitaxy, films are thought to grow on graphene-covered substrates with epitaxial registry to the substrate, due to the “remote” lattice potential of the substrate potential that permeates through graphene [1,7]. Applications include lattice-mismatched epitaxy with reduced dislocation densities [8,9], etch-free exfoliation of membranes for flexible electronics and reuse of substrates [1], and the discovery of new properties induced by extreme strain and strain gradients in membranes [10–12].

A fundamental challenge, however, is controlling the film stoichiometry during growth on graphene. Due to the weak van der Waals interactions, the sticking coefficients σ for metals on multilayer graphite are typically $\sigma < 0.1$ at room temperature as measured by desorption spectroscopy [13], x-ray photoemission spectroscopy (XPS) [14,15], and scanning tunneling microscopy (STM) [14,15]. This lies in stark contrast with the typical $\sigma \sim 1$ for metals on semiconductor, oxide, and metal surfaces [16], which enables a simple one-to-one correspondence between film stoichiometry and incident flux ratios. Although σ on monolayer graphene-covered surfaces is anticipated to be closer to unity [16], due to the “remote” substrate interactions that permeate through graphene [1,7,17], sticking on graphene is less understood and unlikely to be exactly 1. Moreover, the “remote” argument suggests that σ on graphene-covered substrates should depend on the identity of the substrate. The impact of element-

dependent, nonunity sticking coefficients during growth on monolayer graphene is generally overlooked, in part, because remote epitaxy has focused on compound semiconductors such as GaAs for which the stoichiometry is self-limited by growth within an adsorption-controlled window [18,19]. But for more complex materials such as ternary transition metal oxides or intermetallic Heusler compounds, adsorption-controlled growth windows are only accessible in select cases [2,20–23]. Controlling the stoichiometry of these materials during remote epitaxy or van der Waals epitaxy on graphene [2,5,10,12,24–26] in the ultrathin limit will require understanding the sticking coefficients on graphene.

Here, using MBE growth of the magnetic shape memory alloy Ni_2MnGa , we show that the sticking coefficients for transition metals on graphene-covered substrates are nonunity and both element and temperature dependent. Our measurements of the stoichiometry by ion backscattering spectrometry (IBS) and energy-dispersive spectroscopy (EDS) for films with thicknesses 20–80 nm provide upper bounds for the sticking coefficients of Ni and Mn on graphene/ MgO , which are less than 0.65 at 600–625 °C. Controlling the stoichiometry requires compensating for the nonunity sticking coefficient on graphene, or initiating growth at low temperatures where σ on graphene is near unity. We demonstrate epitaxial Ni_2MnGa films that can be mechanically exfoliated, and show how externally applied strain in Ni_2MnGa membranes tunes the magnetic coercive field.

II. RESULTS AND DISCUSSION

Ni_2MnGa films were grown by molecular beam epitaxy (MBE) on graphene-covered MgO (001) substrates. The graphene was grown by chemical vapor deposition on polycrystalline Cu foils and wet transferred to the MgO (001)

^{*}jkawasaki@wisc.edu

substrate using a poly(methyl methacrylate) (PMMA) handle, Cu etch, and scoop from de-ionized water, as described in Refs. [5,10]. Films with a nominal composition Ni_2MnGa and nominal thickness 20–80 nm were grown by MBE using elemental effusion cell sources, with typically fluxes of 2.2×10^{13} atoms/($\text{cm}^2 \text{ s}$) for Ni and 1.1×10^{13} atoms/($\text{cm}^2 \text{ s}$) each for Mn and Ga. We use the term “nominal” to indicate the composition and thickness if all of the incident Ni, Mn, and Ga atomic fluxes stuck to the surface ($\sigma = 1$). All samples were capped with ~ 20 nm of Au at room temperature before removal from the MBE system, to avoid oxidation. Fluxes were measured *in situ* using a quartz crystal microbalance and calibrated to absolute fluxes via *ex situ* ion backscattering spectrometry (IBS) measurements on calibration samples, grown at room temperature on Si. Energy-dispersive x-ray spectroscopy (EDS, beam energy 10–20 keV, interaction depth of a few microns) was used to measure the relative differences in Ni_2MnGa film composition. The increased depth sampling of IBS and EDS, compared to more surface-sensitive XPS, allows us to sum over all species that stick, including those that may intercalate [27–29] or diffuse [30,31] beneath graphene, rather than primarily detecting species that reside at the surface.

Figure 1(a) compares IBS measurements (He^+ , 4.9 MeV, $\theta = 8^\circ$) of a nominally 20-nm-thick Ni_2MnGa film grown on graphene/MgO with a film grown directly on MgO. Growth was performed at 600°C on an MgO substrate that is half covered with graphene, such that both sides of the sample are exposed to the same incident atomic fluxes of Ni, Mn, and Ga. We find that the areal density of Ga on graphene/MgO and on MgO are nearly equal. In contrast, the areal densities of Ni and Mn on graphene/MgO are only $\sim 40\%$ – 80% of the Ni and Mn on the MgO surface. Similar results are found for EDS measurements of thicker films. Figure 1(b) compares EDS measurements for nominally 80-nm-thick Ni_2MnGa films grown on graphene/MgO and MgO at 625°C , where again we observe similar sticking for Ga on the graphene/MgO and MgO sides, and a $\sim 50\%$ reduction of the sticking for Ni and Mn on graphene/MgO compared to MgO.

The large stoichiometry differences in films with nominal thicknesses 20–80 nm are at first surprising, since differences in the sticking coefficient are expected to be limited to within the first few atomic layers of growth. For planar film growth, after a layer of Ni_2MnGa covers the graphene or MgO surface, subsequent Ni_2MnGa film growth in both cases should be Ni_2MnGa on Ni_2MnGa , and thus the stoichiometries of thick films should converge.

We attribute the large observed stoichiometry differences to a combination island morphology and reduced sticking coefficients on graphene. Scanning electron micrographs (SEM) reveal that the nominally 80-nm-thick film grown on graphene/MgO at 625°C has a disconnected island morphology [Fig. 1(f)], which we attribute to poor wetting on low surface energy graphene. Similar poor wetting and three-dimensional island growth has been observed for other films on monolayer graphene-covered surfaces, including GaAs on graphene/Si [32], Mn on graphene/Ge [30], and several elemental metals on monolayer graphene/SiC [33]. This poor wetting of metals on graphene has been attributed to the low adsorption energies of many metals (including Ni and Mn)

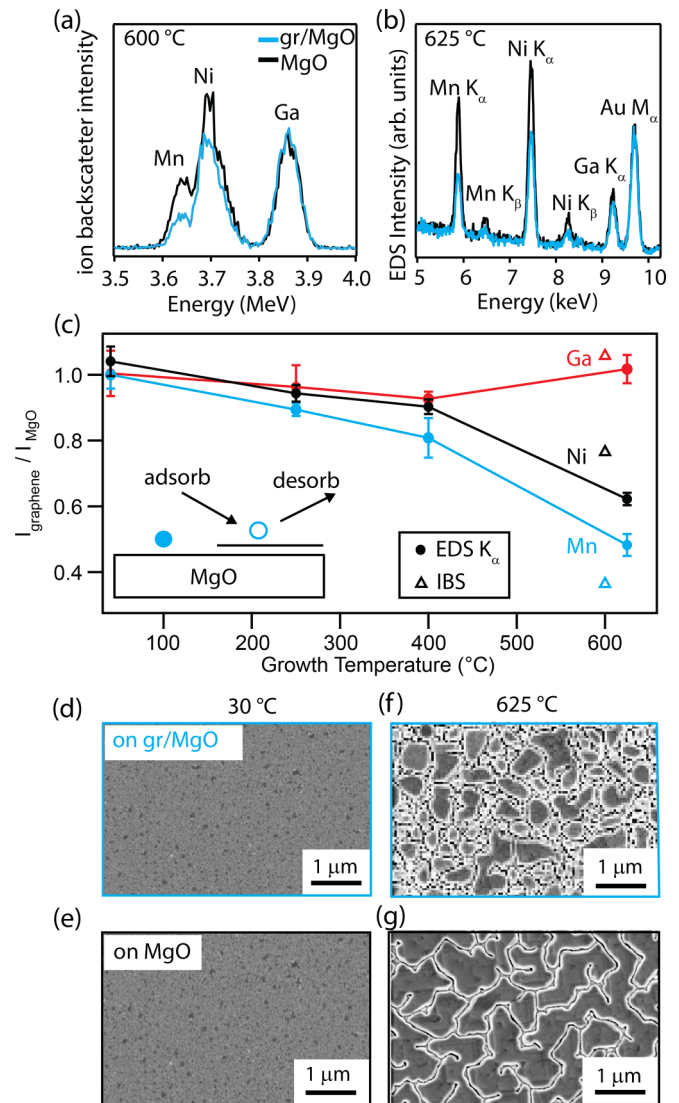


FIG. 1. (a) Ion beam scattering (IBS) for nominally 20-nm-thick Ni_2MnGa films grown on graphene/MgO and MgO at 600°C , showing reduced sticking for Ni and Mn on graphene. (b) Energy-dispersive x-ray spectroscopy (EDS) measurements for Ni_2MnGa films with a nominal thickness 80 nm on graphene/MgO and on MgO. Both the IBS and EDS samples were capped with a protective layer of Au. Data are normalized to the incident ion or electron beam fluxes, respectively. (c) EDS (solid circles) and IBS (open triangles) intensity ratios $I_{\text{graphene}}/I_{\text{MgO}}$, tracking temperature- and element-dependent changes in the cumulative sticking coefficient for Ni_2MnGa on graphene-covered MgO. Error bars are standard deviations on at least five different regions of a given sample. (d), (e) SEM images of the nominally 80-nm-thick films grown at room temperature on graphene/MgO and MgO and capped with Au. (f), (g) SEM images of the nominally 80-nm-thick films grown at 625°C on graphene/MgO and MgO and capped with Au.

on graphene compared to their cohesive energies [33]. In contrast, films grown directly on MgO at the same temperature have a smoother and more connected morphology [Fig. 1(g)]. This morphology on graphene suggests that even after tens of nanometers of nominal growth, some exposed regions of the graphene remain. Thus our IBS and EDS measurements

result from combined sticking on exposed graphene regions (where $\sigma < 1$) and on Ni_2MnGa islands (where $\sigma \sim 1$). This cumulative sticking coefficient σ' is therefore an upper bound for the true sticking coefficient σ on graphene in the atomic layer limit.

Importantly, we find the cumulative sticking on graphene/MgO is highly temperature and element dependent. Figure 1(c) (solid circles) plots the EDS intensity ratio on the graphene/MgO versus on MgO ($I_{\text{graphene}}/I_{\text{MgO}}$), for a series of nominally 80-nm-thick Ni_2MnGa films as a function of growth temperature. We normalize to the intensity on the MgO side, since the sticking coefficients for metals directly on MgO are nominally 1. Thus the ratio $I_{\text{graphene}}/I_{\text{MgO}}$ is approximately equal to the cumulative sticking coefficient on graphene/MgO. Cumulative sticking for Ni and Mn on graphene/MgO is lowest at a high substrate temperature and approaches 1 for all three elements below 400 °C. We attribute this temperature dependence on graphene to the combined decreased desorption rate and smoother morphology with less exposed graphene at a lower temperature [Fig. 1(d)]. We attribute the reduced sticking on graphene, compared to MgO, to relatively weak van der Waals interactions between metal adsorbates and graphene. Indeed, density functional theory calculations suggest that adsorption energies for metals on graphene are of order $E_a \sim 0.5$ eV, compared to $E_a \sim 3$ eV for Au on the Au (111) surface [16]. Surprisingly, the sticking coefficient for Ga on graphene is near unity and independent of temperature, despite the fact that Ga has a higher vapor pressure than Ni and a similar vapor pressure as Mn. We speculate the increased sticking of Ga on graphene may arise from reactions or from intercalation beneath graphene. Ga, In, and Sn are known to intercalate at graphene/SiC interfaces [27], and Au is known to intercalate between sheets of graphite [28]. The IBS measurement for the 20-nm sample grown at 600 °C (open triangles) is consistent with these trends, but we caution that this IBS sample was thinner than the 80-nm EDS samples, and there is likely a thickness dependence as the exposed graphene regions become covered with film.

Our findings suggest that control of the Ni_2MnGa film stoichiometry on graphene requires compensating for the nonunity sticking coefficients at high growth temperatures or initiating the growth at lower temperatures where the cumulative sticking coefficients are closer to 1. Lower-temperature growth is also beneficial for promoting a smoother morphology on graphene [Fig. 1(d)], since the kinetic processes that lead to dewetting and island growth are suppressed at lower temperature [34]. Once the interface has formed and the graphene layer is buried, growth can resume under more normal temperatures and fluxes.

For simplicity we adopt the strategy of growth at a fixed lower temperature. Figure 2 compares x-ray diffraction patterns for Ni_2MnGa films grown at 370, 400, and 600 °C on graphene/MgO, with a film grown by directly on MgO. We find that the sample grown at 600 °C on graphene/MgO displays several impurity reflections, marked by an “x,” consistent with large deviations from stoichiometry observed by IBS and EDS (Fig. 1). Films grown at 400 °C and below on graphene display only the Heusler Ni_2MnGa reflections and no impurity reflections. Interestingly, the films

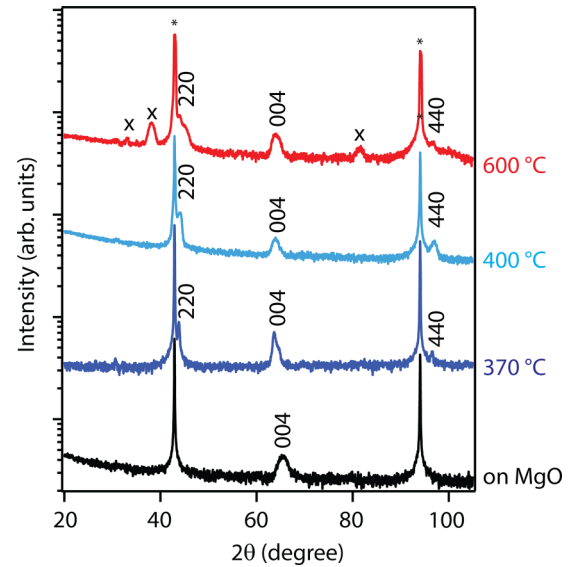


FIG. 2. Out-of-plane x-ray diffraction scans ($\text{Cu } K\alpha$) of Ni_2MnGa films grown on MgO and on graphene/MgO at 600, 400, and 370 °C, compared to film grown directly on MgO. Asterisks * denote MgO substrate reflections and “x” denotes secondary phase reflections.

on graphene/MgO display both $00L$ and $HH0$ reflections, indicating both (001)- and (110)-oriented growth, whereas epitaxy directly on MgO produces only (001)-oriented growth (black curve).

Azimuthal ϕ scans reveal that both (110)- and (001)-oriented Ni_2MnGa domains on graphene/MgO (001) have well-defined in-plane orientations with respect to the underlying MgO substrate, despite the presence of the polycrystalline graphene interlayer. In Fig. 3(a), the fourfold pattern of Ni_2MnGa 101 reflections is rotated by 45° with respect to MgO 101. This indicates that the (001) Ni_2MnGa domain has a 45° rotated cube on a cube epitaxial relationship to MgO, i.e., Ni_2MnGa (001) [110] \parallel MgO (001) [100], and a 2% tensile lattice mismatch [Fig. 3(b)]. For the (110) domain, we observe a fourfold pattern of 010 Ni_2MnGa reflections aligned with the MgO 101. This indicates two rectangular domains, labeled A and B, with orientations Ni_2MnGa (110) [001] \parallel MgO (001) [010] and Ni_2MnGa (110) [001] \parallel MgO (001) [100] [Fig. 3(b)]. For these (110)-oriented domains, the mismatch between Ni_2MnGa d_{110} and the MgO a lattice spacings is 2%, while the mismatch in the orthogonal in-plane direction ($a_{\text{Ni}_2\text{MnGa}}$ vs a_{MgO}) is much larger and would require a larger supercell to produce a commensurate structure. We speculate that the presence of the graphene interlayer may relax the constraints of direct epitaxy in which there are direct bonds formed between the film and substrate, and allow for alternative film orientations that lower the total energy. Similar new epitaxial structures have been observed in the form of rotated superstructures for GdPtSb films on graphene/sapphire [5]. Further studies are required to understand why the (110) domain appears on graphene/MgO and not directly on MgO.

Finally, we show that applying external strains to exfoliated membranes tunes the magnetic properties. We exfoliate membranes by adhering the film to a glass slide using a

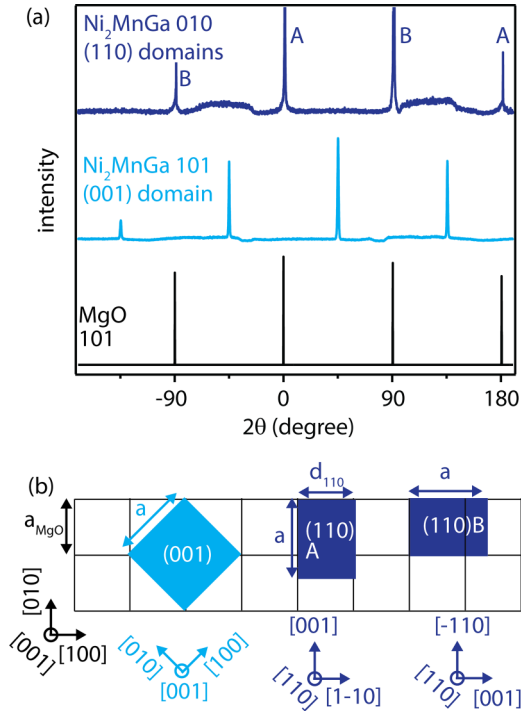


FIG. 3. (a) Azimuthal ϕ scans for a Ni_2MnGa film grown on graphene/MgO (001). The off-axis 010 reflections track the in-plane orientation of Ni_2MnGa domains with (110) out-of-plane orientation. The 101 reflections track the in-plane orientation of the (001) domain. (b) Domain orientations of Ni_2MnGa (blue) with respect to MgO (001) (black) determined from (a).

crystal bond, then peeling the film from the graphene/MgO. After exfoliation we observe only the 110- and 001-type film reflections and no substrate reflections, as shown in Fig. 4(a). We then apply ripples to the membrane to induce strain. The rippling was performed by adhering a tensile strained polyurethane film to the exfoliated Ni_2MnGa membrane, heating to approximately 150°C to release the Ni_2MnGa /polyurethane bilayer from the crystal bond, and relaxing to impart ripples upon contraction of the polyurethane. Further details of the rippling procedure are described in Ref. [10].

Figure 4(b) shows superconducting quantum interference device (SQUID) magnetometry measurements for a Ni_2MnGa film on graphene/MgO, and the same film after exfoliation and subjected to strain in the form of rippling, measured at 100 K with the field oriented in plane. We find that strain and/or strain gradients enhance the coercive field, from 400 to 650 Oe. The membrane has a thickness 80 nm, ripple period of 8 μm , and a peak-to-peak height of 3 μm . Assuming a sinusoidal shape we estimate the peak magnitudes of strain to be $|\epsilon| < 3.6\%$, if there is no plastic deformation [10]. The strain-tunable coercive field may be useful for strain-assisted reading and writing of magnetic memory.

III. CONCLUSIONS

In summary, we showed that sticking coefficients for metals on graphene-covered substrates are nonunity and highly

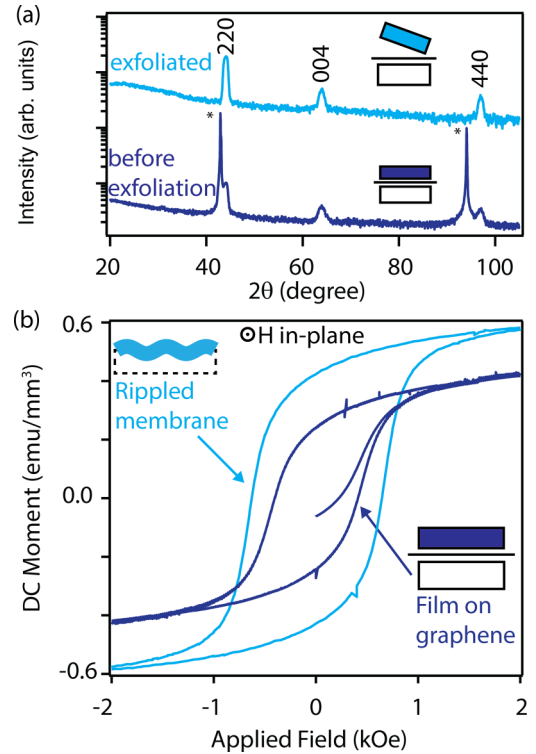


FIG. 4. (a) X-ray diffraction before and after membrane exfoliation. (b) SQUID magnetometry of a relaxed Ni_2MnGa film on graphene/MgO (dark blue), and on the same sample after exfoliation and rippling to create a strained Ni_2MnGa membrane (light blue). The measurement was performed at 100 K with the field oriented within the film plane.

dependent on element and temperature. IBS and EDS measurements of films with tens of nanometers thickness provide upper bounds for the sticking coefficients on graphene/MgO: $\sigma < 0.65$ for Ni and Mn and $\sigma \sim 1$ for Ga at $600\text{--}625^\circ\text{C}$. Surface-sensitive measurements in the monolayer limit are required to fully quantify the atomic sticking coefficients on graphene, and understand the effects of changing the underlying substrate and effects of defects and contaminants at the graphene/substrate interface. In particular, the lattice potential permeation argument of remote epitaxy [6,7] suggests that the sticking coefficients should also depend on the identity of the substrate. We show that synthesis at a lower temperature $\leq 400^\circ\text{C}$ enables a phase-pure epitaxy of Ni_2MnGa films on graphene/MgO. Similar strategies may apply to remote and van der Waals epitaxy of other materials with complex stoichiometries, for which adsorption-controlled growth windows are not accessible.

ACKNOWLEDGMENTS

We thank Greg Haugsted for IBS/Rutherford backscattering spectrometry (RBS) measurements. This work was primarily supported by the Air Force Office of Scientific Research Grant No. FA9550-21-0127 (Z.L. and J.K.K.). Preliminary Heusler synthesis was supported by the National Science Foundation DMR-1752797 (Z.L., S.M., and J.K.K.). Graphene synthesis via chemical vapor deposition (CVD)

was supported by the U.S. Department of Energy, Office of Science, Basic Energy Sciences, Grant No. DE-SC0016007 (K.S. and M.S.A.). We gratefully acknowledge the use of

x-ray diffraction facilities supported by the NSF through the University of Wisconsin Materials Research Science and Engineering Center under Grant No. DMR-1720415.

-
- [1] Y. Kim, S. S. Cruz, K. Lee, B. O. Alawode, C. Choi, Y. Song, J. M. Johnson, C. Heidelberger, W. Kong, S. Choi *et al.*, *Nature (London)* **544**, 340 (2017).
- [2] H. Yoon, T. K. Truttman, F. Liu, B. E. Matthews, S. Choo, Q. Su, V. Saraswat, S. Manzo, M. S. Arnold, M. E. Bowden *et al.*, *Sci. Adv.* **8**, eadd5328 (2022).
- [3] A. Koma, *Thin Solid Films* **216**, 72 (1992).
- [4] F. Ren, B. Liu, Z. Chen, Y. Yin, J. Sun, S. Zhang, B. Jiang, B. Liu, Z. Liu, J. Wang *et al.*, *Sci. Adv.* **7**, eabf5011 (2021).
- [5] D. Du, T. Jung, S. Manzo, Z. LaDuca, X. Zheng, K. Su, V. Saraswat, J. McChesney, M. S. Arnold, and J. K. Kawasaki, *Nano Lett.* **22**, 8647 (2022).
- [6] J. Kim, C. Bayram, H. Park, C.-W. Cheng, C. Dimitrakopoulos, J. A. Ott, K. B. Reuter, S. W. Bedell, and D. K. Sadana, *Nat. Commun.* **5**, 4836 (2014).
- [7] W. Kong, H. Li, K. Qiao, Y. Kim, K. Lee, Y. Nie, D. Lee, T. Osadchy, R. J. Molnar, D. K. Gaskill *et al.*, *Nat. Mater.* **17**, 999 (2018).
- [8] S.-H. Bae, K. Lu, Y. Han, S. Kim, K. Qiao, C. Choi, Y. Nie, H. Kim, H. S. Kum, P. Chen *et al.*, *Nat. Nanotechnol.* **15**, 272 (2020).
- [9] B. Liu, Q. Chen, Z. Chen, S. Yang, J. Shan, Z. Liu, Y. Yin, F. Ren, S. Zhang, R. Wang *et al.*, *Nano Lett.* **22**, 3364 (2022).
- [10] D. Du, S. Manzo, C. Zhang, V. Saraswat, K. T. Genser, K. M. Rabe, P. M. Voyles, M. S. Arnold, and J. K. Kawasaki, *Nat. Commun.* **12**, 2494 (2021).
- [11] D. Du, J. Hu, and J. K. Kawasaki, *Appl. Phys. Lett.* **122**, 170501 (2023).
- [12] H. S. Kum, H. Lee, S. Kim, S. Lindemann, W. Kong, K. Qiao, P. Chen, J. Irwin, J. H. Lee, S. Xie *et al.*, *Nature (London)* **578**, 75 (2020).
- [13] J. Arthur and A. Cho, *Surf. Sci.* **36**, 641 (1973).
- [14] I. Lopez-Salido, D. C. Lim, and Y. D. Kim, *Surf. Sci.* **588**, 6 (2005).
- [15] A. R. Howells, L. Hung, G. S. Chottiner, and D. A. Scherson, *Solid State Ionics* **150**, 53 (2002).
- [16] D. Appy, H. Lei, C.-Z. Wang, M. C. Tringides, D.-J. Liu, J. W. Evans, and P. A. Thiel, *Prog. Surf. Sci.* **89**, 219 (2014).
- [17] J. Rafiee, X. Mi, H. Gullapalli, A. V. Thomas, F. Yavari, Y. Shi, P. M. Ajayan, and N. A. Koratkar, *Nat. Mater.* **11**, 217 (2012).
- [18] J. Arthur, Jr., *J. Appl. Phys.* **39**, 4032 (1968).
- [19] A. Cho and J. Arthur, *Prog. Solid State Chem.* **10**, 157 (1975).
- [20] B. Jalan, P. Moetakef, and S. Stemmer, *Appl. Phys. Lett.* **95**, 032906 (2009).
- [21] J. F. Ihlefeld, W. Tian, Z.-K. Liu, W. A. Doolittle, M. Bernhagen, P. Reiche, R. Uecker, R. Ramesh, and D. G. Schlom, *IEEE Trans. Ultrason. Ferroelectr. Freq. Control* **56**, 1528 (2009).
- [22] C. D. Theis, J. Yeh, D. G. Schlom, M. Hawley, and G. Brown, *Thin Solid Films* **325**, 107 (1998).
- [23] E. H. Shourov, R. Jacobs, W. A. Behn, Z. J. Krebs, C. Zhang, P. J. Strohbeen, D. Du, P. M. Voyles, V. W. Brar, D. D. Morgan *et al.*, *Phys. Rev. Mater.* **4**, 073401 (2020).
- [24] C.-H. Ma, L.-S. Lu, H. Song, J.-W. Chen, P.-C. Wu, C.-L. Wu, R. Huang, W.-H. Chang, and Y.-H. Chu, *APL Mater.* **9**, 051115 (2021).
- [25] R. Jia, H. S. Kum, X. Sun, Y. Guo, B. Wang, P. Fang, J. Jiang, D. Gall, T.-M. Lu, M. Washington *et al.*, *J. Vac. Sci. Technol. A* **39**, 040405 (2021).
- [26] L. Dai, J. Zhao, J. Li, B. Chen, S. Zhai, Z. Xue, Z. Di, B. Feng, Y. Sun, Y. Luo *et al.*, *Nat. Commun.* **13**, 2990 (2022).
- [27] N. Briggs, B. Bersch, Y. Wang, J. Jiang, R. J. Koch, N. Nayir, K. Wang, M. Kolmer, W. Ko, A. De La Fuente Duran *et al.*, *Nat. Mater.* **19**, 637 (2020).
- [28] I. Gierz, T. Suzuki, R. T. Weitz, D. S. Lee, B. Krauss, C. Riedl, U. Starke, H. Höchst, J. H. Smet, C. R. Ast *et al.*, *Phys. Rev. B* **81**, 235408 (2010).
- [29] L. B. Ebert, *Annu. Rev. Mater. Sci.* **6**, 181 (1976).
- [30] P. J. Strohbeen, S. Manzo, V. Saraswat, K. Su, M. S. Arnold, and J. K. Kawasaki, *ACS Appl. Mater. Interfaces* **13**, 42146 (2021).
- [31] W. K. Morrow, S. J. Pearton, and F. Ren, *Small* **12**, 120 (2016).
- [32] Y. Alaskar, S. Arafin, D. Wickramaratne, M. A. Zurbuchen, L. He, J. McKay, Q. Lin, M. S. Goorsky, R. K. Lake, and K. L. Wang, *Adv. Funct. Mater.* **24**, 6629 (2014).
- [33] X. Liu, C.-Z. Wang, M. Hupalo, H.-Q. Lin, K.-M. Ho, and M. C. Tringides, *Crystals* **3**, 79 (2013).
- [34] D. McDougall, H. Hattab, M. Hershberger, M. Hupalo, M. H. von Hoegen, P. Thiel, and M. Tringides, *Carbon* **108**, 283 (2016).